A panoramic coded aperture gamma camera for radioactive hotspots localization

V. Paradiso, K. Amgarou, N. Blanc De Lanaute, Vincent Schoepff, Guillaume Amoyal, C. Mahe, O. Beltramello, E. Liénard

Journal of Instrumentation

SISSA

OPEN ACCESS

A panoramic coded aperture gamma camera for radioactive hotspots localization

To cite this article: V. Paradiso *et al* 2017 *JINST* **12** P11010

Jinst

Published by IOP Publishing for Sissa Medialab

Received: *October 6, 2017*
Accepted: *October 24, 2017*
Published: *November 13, 2017*

A panoramic coded aperture gamma camera for radioactive hotspots localization

V. Paradiso,[a,b,1] **K. Amgarou,**[c] **N. Blanc De Lanaute,**[d] **V. Schoepff,**[e] **G. Amoyal,**[e] **C. Mahe,**[c] **O. Beltramello**[b] **and E. Liénard**[f]

[a] *Mirion Technologies (CANBERRA), 78182 St-Quentin-en-Yvelines, France*
[b] *CERN, Experimental Physics Department, ATLAS Detector Operation, Geneva 23, CH-1211, Switzerland*
[c] *CEA, DEN, 30207 Bagnols-sur-Céze, Marcoule, Franc*
[d] *Mirion Technologies (CANBERRA), 37600 Loches, France*
[e] *CEA, LIST, 91191 Gif-sur-Yvette, France*
[f] *Normandie Univ, ENSICAEN, UNICAEN, CNRS/IN2P3, LPC Caen, 14000 Caen, France*

E-mail: enzo.paradiso@cern.ch

Abstract: A known disadvantage of the coded aperture imaging approach is its limited field-of-view (FOV), which often results insufficient when analysing complex dismantling scenes such as post-accidental scenarios, where multiple measurements are needed to fully characterize the scene.

In order to overcome this limitation, a panoramic coded aperture γ-camera prototype has been developed. The system is based on a 1 mm thick CdTe detector directly bump-bonded to a Timepix readout chip, developed by the Medipix2 collaboration (256×256 pixels, 55 µm pitch, $14.08 \times 14.08\,\mathrm{mm}^2$ sensitive area). A MURA pattern coded aperture is used, allowing for background subtraction without the use of heavy shielding. Such system is then combined with a USB color camera. The output of each measurement is a semi-spherical image covering a FOV of 360 degrees horizontally and 80 degrees vertically, rendered in spherical coordinates (θ,ϕ). The geometrical shapes of the radiation-emitting objects are preserved by first registering and stitching the optical images captured by the prototype, and applying, subsequently, the same transformations to their corresponding radiation images.

Panoramic gamma images generated by using the technique proposed in this paper are described and discussed, along with the main experimental results obtained in laboratories campaigns.

Keywords: Search for radioactive and fissile materials; Dosimetry concepts and apparatus; Image processing

[1] Corresponding author.

https://doi.org/10.1088/1748-0221/12/11/P11010

2017 JINST 12 P11010

Contents

1 Introduction **1**

2 Material and methods **2**
2.1 A portable panoramic gamma imaging camera 2
2.2 Multimodal image stitching pipeline overview 4
2.2.1 Optical image registration 5
2.2.2 Radiation image stitching 6

3 Results and discussion **7**
3.1 Radiation image stitching with planar sources 7
3.1.1 Combining multiple planar sources 9
3.2 Panoramic images with planar and point sources 12

4 Conclusion **13**

2017 JINST 12 P11010

1 Introduction

Localization of radioactive sources or hotspots is a major issue for radiological safety of operators in nuclear facilities. For this purpose, portable gamma imaging systems allow remote localization of radioactive sources from greater distances than conventional rate meters, leading to significant reductions of the dose received by operators.

Nowadays, portable *coded aperture* gamma cameras for industrial applications [2, 12, 14, 16, 23, 29, 39] are undergoing impressive developments and improvements in terms of lightness, usability, response sensitivity, angular resolution, and spectrometric capabilities. However, a drawback of the coded aperture imaging approach is its limited FOV [10]. For this reason, a method for combining multiple radiation images preserving though the geometrical shape of the associated radioactive sources has been designed and tested.

The need to combine two or more images into a single larger image has arisen in a number of contexts not that recently. Back in 1979, for example, mosaics of Jupiter and Saturn have been generated by using multiple images captured from the cameras aboard the Voyager 1 and Voyager 2 spacecrafts [34, 35]. Today, such process is usually referred to as *image stitching*, which can be thought of as a method consisting of three main phases: *image registration*, *image reprojection*, and *image compositing*. During the image registration phase, portions of adjacent images are compared to find the transformations so that, roughly speaking, the points in one image can be related to their corresponding points in the other. Once the images have been registered, they are reprojected according to the transformations found in the previous step. Finally, the image compositing phase consists in merging the registered images in order to mitigate the transition colour discontinuities between adjacent stitched images, typically referred to as *seams*.[1]

[1] A seam is the artificial edge generated by the intensity differences of pixels immediately next to where the images are merged.

An impressive amount of investigation has been conducted in the medical imaging field concerning image registration of multimodal images [8, 21, 27, 30], as a component of a wide number of applications, ranging from diagnostic to areas such as surgical and radiotherapeutic procedures. However, contrarily to the instruments used in medical imaging (e.g. positron emission tomography and magnetic resonance imaging), images generated by portable γ-cameras do not yet necessarily provide a sufficient spacial resolution and amount of visual details required for performing *image registration* using *only* radiation images. This is mainly due to the impossibility of retrieving distinctive features for using robust local descriptors concerning the radiation-emitting sources found, such as accurate global intensity variations in different radiation images regarding the same point on a given surface, the accurate shape of the edges and corners of the radioactive object, boundary regions, and so on.

Some work has been done in the past concerning panoramic radiation images generated by γ-cameras for nuclear power plants and radiation facilities [36]. However, in such work multiple pixelated detectors modules and several masks were adopted to generate a panorama image, and the preservation of the geometrical shape of the radiation-emitting objects was not considered.

The overall procedure here proposed uses only one Timepix detector and one optical camera (more details regarding the prototype are provided in section 2.1), and consists of two main phases: the acquisition phase, where all optical images are *autonomously* acquired as well as their superimposed γ-images, and the processing phase, where the optical and radiation images are coherently stitched together.

In the remainder of this paper, section 2.1 provides an overview of the prototype developed for this study. In section 2.2, the algorithms designed for automatically combining optical and radiation images into a final coherent panorama image with a 360° FOV are described. In section 3, the associated methods are discussed along with their validation, namely with point and planar radioactive sources made available by two CEA laboratories.[2]

2 Material and methods

2.1 A portable panoramic gamma imaging camera

The prototype developed for this study is an embedded gamma camera comprising a Timepix chip [24] directly bump-bounded to a 1 mm-thick cadmium telluride (CdTe) semiconductor substrate. CdTe is a II-VI compound semiconductor material with atomic numbers of 48 (Cd) and 52 (Te), a wide band gap of 1.44 eV, a high density (ρ = 5.85 g/cm^3), and a high resistivity ($\geq 10^9\,\Omega\,$cm) [4, 38]. Such properties allow the capability of operation of the detector at room temperature, and thus of the γ-camera as well.

Similarly to the iPIX γ-camera, whose performance and main aspects are analysed by some of us in [2], the system employs a tungsten coded aperture [11], providing two mask ranks (figure 1) and three different thicknesses. More specifically, masks are classified according to their rank and thickness: R7e4, R7e8, and R13e2. The label *e* is an abbreviation of the word "*épaisseur*" (a French translation of "thickness"), expressed in mm. The planar area of such apertures is four times that of the CdTe detector used, and their patterns were designed according to the MURA arrays [17].

[2]The "*Laboratoire simulation et techniques de démantèlement nucléaire*", at Marcoule, and the "*Laboratoire d'Intégration de Systèmes et des Technologies*", at Saclay.

2017 JINST 12 P11010

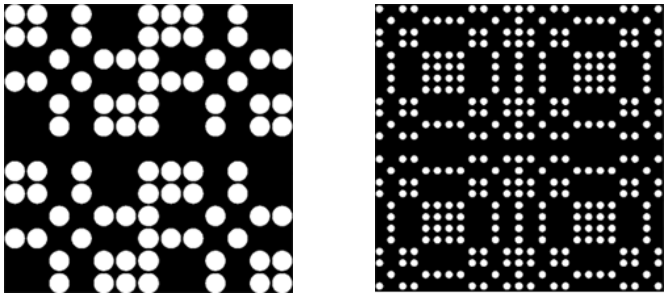

(a) Rank 7. **(b)** Rank 13.

Figure 1. Pattern designs for the coded aperture masks used.

For this study, the Logitech C920 optical camera was adopted and integrated with the prototype. Moreover, in order to perform panoramic measurements without requiring any physical interaction between operators, the system allows full remote control over data networks, including Wi-Fi, using a motorised pan-tilt device, the FLIR PTU-D46-17 pan-tilt unit. The resulting prototype is shown in figure 2.

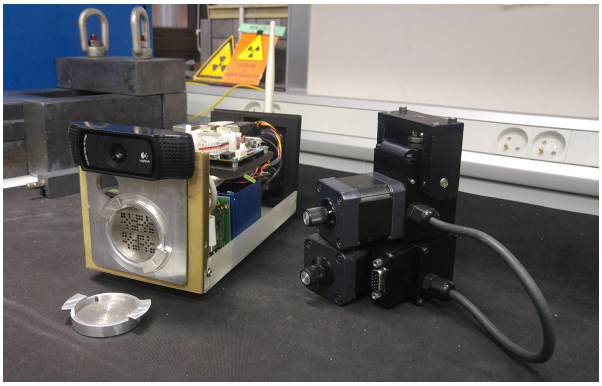

Figure 2. The γ-camera prototype (left) and the motorized pan-tilt unit (FLIR PTU-D46-17) adopted for remotely changing its position and orientation (right). Both γ-camera and pan-tilt unit are completely battery-powered, and no cables are thus required for operating the system.

The prototype developed is completely independent from its client devices used by operators. For this reason, also the acquisition of radiation information is embedded in its computing board, the ODROID-XU4 [28], using the D2XX library for Linux [13], developed by FTDI (Future Technology Devices International) primarily to support direct access in Linux to USB devices, such as the FITPix USB interface [22].

Every pixel of the Timepix sensor is independently configured to run in ToT (Time-over-Threshold) mode: the counter is incremented continuously as long as the pixel output signal is above the pre-set threshold level. The number of clock cycles is counted until the pixel output signal crosses back below this threshold. As described in more detail in [24], the number of clock cycles can be directly related to the voltage amplitude of the pixel output signal.

2017 JINST 12 P11010

The ToT mode of the Timepix chip relies on the configured shutter time, during which the counter is incremented, continuously, while the input charge is over threshold. When this shutter time ends, pixel values are retrieved from the buffer and cleared. The process is repeated for the duration of the measurement (i.e. until the chosen number of frames is reached).

Once the acquisition is completed and the corresponding frames returned by the Timepix chip are collected and stored, the corresponding matrices are provided as input to the processing algorithm of the prototype, which is the same that is used by the iPIX gamma camera when performing a single measurement (i.e. not panoramic). Consequently, in such case, performances of the gamma camera in terms of sensitivity and angular resolution are comparable to those of iPIX, widely documented in [2]. Nevertheless, one of the key differences of the prototype respect to iPIX consists in the capability to perform *panoramic measurements*. That is, the ability to locate sources of gamma radiation within a 360° FOV, and to render the resulting images via spherical projection. For this reason, when performing panoramic measurements, the algorithm implemented for this study performs a further step when processing radiological information, which is described in section 2.2.

2.2 Multimodal image stitching pipeline overview

Approaches for generating panoramic images by means of only one camera use often human interaction or other specific restrictions during the image sources acquisition stage [3].

In our context though, as the use of the prototype is foreseen in environments that can be potentially highly radioactive during both planned and emergency interventions, also the acquisition phase of optical and radiation images has been automated, by sequentially capturing all optical images using the motorized pan-tilt unit and acquiring and processing, meanwhile, the respective radiation information. For this reason, all images are labelled depending on their order while being captured by the camera. This significantly eases the process, as each optical image is thus compared and matched only to the one that is adjacent, and whose is already known having an overlapping area. Such region is proportional to the angle of rotation of the pan-tilt device (angle per step), pre-set as parameter in the implementation code of the prototype.

More specifically, depending on the *vertical* FOV of the final panorama image, a number of optical frames are vertically acquired and then stitched together using the algorithm described below (figure 3a) in the present section. Once the 360° *horizontal* FOV has been covered, each vertical result obtained in the first phase is an input for the final horizontal stitching phase (figure 3b).

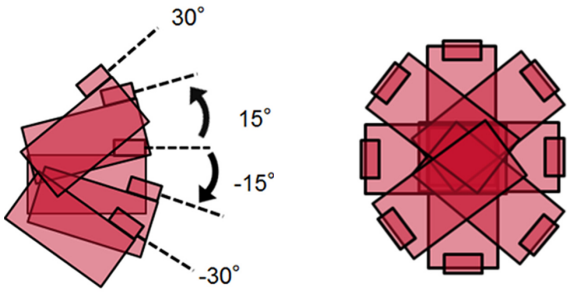

(a) First phase. **(b)** Second phase.

Figure 3. Illustration of the two automated main acquisition phases with the prototype of the optical images to be stitched.

2.2.1 Optical image registration

Algorithms for registering optical images (i.e. the first main phase of image stitching in our context) are among the oldest and most widely known algorithms in Computer Vision. Back in 1981, Lucas and Kanade proposed one of the most currently known registration techniques [26]. Still up to this day, several methods and video compression schemes as important as the ones used by MPEG and H.264 [31], for example, are deeply inspired by such technique.

Given two images acquired by a camera rotated about its centre, the basic geometry of the registration of two images consists in estimating their homography, **H**, which is a linear transformation on homogeneous 3-vectors represented by a non-singular 3×3 matrix [20], which can be described as follows:

$$\begin{pmatrix} x_1' \\ x_2' \\ x_3' \end{pmatrix} = \begin{bmatrix} h_{11} & h_{12} & h_{13} \\ h_{21} & h_{22} & h_{23} \\ h_{31} & h_{32} & h_{33} \end{bmatrix} \begin{pmatrix} x_1 \\ x_2 \\ x_3 \end{pmatrix}, \tag{2.1}$$

or, more briefly, $\mathbf{x}' = \mathbf{H}\,\mathbf{x}$.

As explained in [20], the matrix **H** occurring in this equation may be changed by multiplication by an arbitrary non-zero scale factor without altering the projective transformation. As a reminder, a projective transformation projects every image into another *projectively equivalent* image.[3] For this reason, **H** is a homogeneous matrix, since as in the homogeneous representation of a point, only the ratio of the matrix elements is significant. The interested reader regarding projective geometry and the specializations of projective transformations, such as affine and similarity transformations, is referred to [20] and [15].

Several issues need to be dealt with when stitching images captured from different perspectives and/or at different times, such as blurring or ghosting caused by parallax as well as varying image exposures or other distortions. In our case, we consider the image registration methods typically referred to as *feature-based* [40].

The stitching algorithm of the gamma camera prototype is implemented in C++ using the Open Source Computer Vision Library (OpenCV) [5], made available under a BSD license (Berkeley Software Distribution). The steps that concern the stitching of optical images are inspired by the algorithm proposed by Brown and Lowe [6]. Nevertheless, while in [6] the SIFT algorithm [25] is used to extract and match features between all images, the procedure for feature detection implemented for the gamma camera mainly relies on the computationally more efficient ORB algorithm (Oriented FAST and Rotated BRIEF) [33], which in turn relies on the BRIEF descriptor [7] and FAST keypoint detector [32].

As ORB is a binary string based descriptor, the features found in two adjacent images are then matched by comparing each descriptor of one feature in the first set with all other features in the second set, using the Hamming distance.[4] Although this is not the most computationally efficient approach that could be adopted, it ensures that the best possible matches between adjacent images are found.

[3] That is, leaving all its projective properties invariant.

[4] In Information Theory, the Hamming distance between two strings of equal length is a string metric that can be defined as the minimum number of substitutions required to change one string into the other.

2017 JINST 12 P11010

Once the homography $\mathbf{H}$ has been computed and the correspondences which are consistent are found, the images can be registered and reprojected. Figure 4 shows a result obtained using the algorithm whose main steps are above summarized. This image was acquired and generated using the optical camera of the prototype and its pan-tilt unit. The features of adjacent images were robustly matched and the overall approach yielded a seamless panorama. In this case, the prototype autonomously captured 80 optical frames in order to generate the final panorama image. Using the ODROID-XU4 board of the prototype and its optical camera, the 80 input images were automatically captured in 67 seconds, and they were matched, registered, and composed in 40 seconds, resulting into a final 7234×1681 pixels output panorama, and requiring thus a total time of 107 seconds.

Figure 4. A panorama image with size 7234×1681 pixels captured and generated by the prototype. No radiation sources were present in this case.

2.2.2 Radiation image stitching

During the previous steps of the stitching algorithm above summarized, only optical images (i.e. not superimposed by any γ-image) were considered. Conversely, the presence of radiation information (if any) overlayed on each respective optical image would have led to inconsistencies during such phases.

In case radioactive hotspots are present in the scene under study, the corresponding γ-images can be superimposed only at this stage of the algorithm, since the correct homographies among all pairs of optical images have been already estimated and stored.

For this reason, we apply the homographies retrieved for each pair of adjacent optical images *to their corresponding superimposed radiation images*. More specifically, for each couple of adjacent optical images, I_1 and I_2, the 3×3 homography matrix $\tilde{\mathbf{H}}_{12}$ for registering I_1 with I_2 is applied to their respective superimposed decoded gamma images, $\hat{S}_1$ and $\hat{S}_2$ (the caret $\hat{}$ is used here to indicate that the quantity under it is an estimate). Therefore, if R_v is the overlapping region of I_1 and I_2 (v stands for *visible*), and $R_{\hat{S}}$ is the overlapping region of $\hat{S}_1$ and $\hat{S}_2$ such that:

- $R_{\hat{S}} \neq 0$,
- a radioactive source S is partially or entirely observed in a subset of $R_{\hat{S}}$, and
- such source S refers to the objects visible in the optical images,

we apply $\tilde{\mathbf{H}}_{12}$ also for registering $\hat{S}_1$ with $\hat{S}_2$. This is possible as both gamma images were already previously and consistently superimposed onto I_1 and I_2, respectively, and all images involved are two-dimensional.

2017 JINST 12 P11010

Once the radiation images have been registered (i.e. aligned), if pixels from both $\hat{S}_1$ and $\hat{S}_2$ occur at the same location in the united coordinate system, they need to be *blended* before being overlaid on the correct location of the final stitched panorama, as their intensity may not be exactly the same (similarly to what happens when registering and stitching optical images).

In the context of radiation images, this can be solved by simply computing an *average* value at each pixel:

$$B(\mathbf{x}) = \frac{\sum_k w_k(\mathbf{x})\tilde{S}(\mathbf{x})}{\sum_k w_k(\mathbf{x})}, \tag{2.2}$$

where $\tilde{S}(\mathbf{x})$ are the reprojected γ-images and $w_k(\mathbf{x})$ is 1 at valid pixels and 0 elsewhere, creating in such way a final coherent composite gamma image.

We refer to the process of combining multiple γ-ray images as *radiation image stitching*.

The resulting wider gamma image can be finally superimposed onto the optical stitched image, and the respective result can be rendered. Typically, composed panoramas use a cylindrical [9] or spherical projection [37]. However, any surface adopted for environment mapping in Computer Graphics can be used, including a cube map that represents the full viewing sphere with the six square faces of a box [18].

3 Results and discussion

3.1 Radiation image stitching with planar sources

The response of the gamma camera has been studied using mask R7e4 with the low-activity *planar* sources listed in table 1. To verify their fabrication procedure, a low activity ^{57}Co solution (about 13 kBq/g) was used to prepare the sources and assess their homogeneity using an auto-radiographer (10 min exposure time). The standard deviation obtained was 13% for 10 mm^2 and 9% for 40 mm^2, respectively.

Several configurations and combinations have been experimented, placing the gamma camera at several distances and angles.

Table 1. Low-activity planar sources fabricated and made available by the "Laboratoire de Métrologie de l'Activité Laboratoire National Henri Becquerel" (LNHB) and used in collaboration with CEA LIST.

Units	Radionuclide	Surface activity* (kBq/cm^2)	Nominal activity	Reference date
3	^{57}Co	3.65	429 kBq	30/04/2016
3	^{57}Co	7.37	143 kBq	30/04/2016
3	^{241}Am	3.65	144 kBq	13/01/2015

The first preliminary tests that were carried out involved only one ^{57}Co planar source with 429 kBq activity (see table 1). For example, figures 5 and 6 concern a measurement where the gamma camera prototype was placed at 50 cm from the center of such source, providing a dose rate at the measurement point of ~ 340 nSv/h (measured by means of the CANBERRA instrument Colibri VLD).

2017 JINST 12 P11010

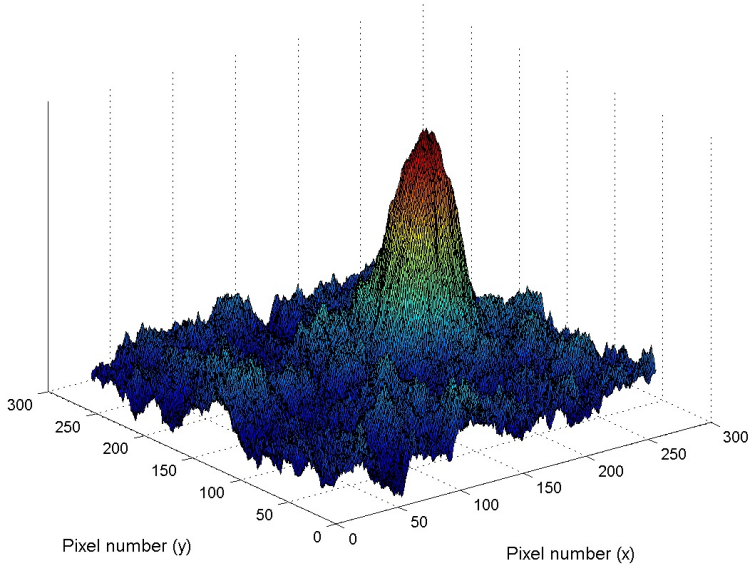

Figure 5. 3-D hotspot profile resulting from a measurement of a planar ^{57}Co source with activity of 429 kBq at 50 cm from the gamma camera, providing an ambient dose equivalent rate of ~ 340 nSv/h at the measurement point.

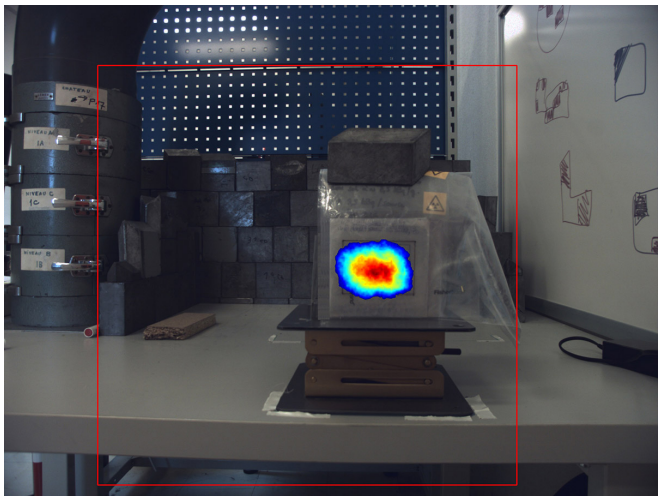

Figure 6. Measurement results obtained with a 429 kBq planar source located at a distance of 50 cm from the γ-camera prototype. For this experiment, 40 frames of 1 sec shutter time were collected, both in mask and antimask position.

The profile of the decoded matrix of figure 5 shows the registered counts associated to each Timepix pixel after the de-convolution process (see [17] and [2] for more details). With this specific configuration, the gamma camera was able to localize the above source with 40 frames of 1 sec shutter time (that is, considering data collection only), both in mask and antimask position.

2017 JINST 12 P11010

3.1.1 Combining multiple planar sources

In order to simulate situations closer to real-life scenarios and to test the algorithm proposed and described in section 2.2, different combinations and configurations have also been experimented using the planar sources listed in table 1.

An example of such experiments consisted in simulating a radioactive surface of rectangular shape, so that its size would exceed the FOV of the gamma camera prototype. In order to achieve this, the sources have been installed at an average distance from the gamma camera of only 16 cm, as follows (see figure 7): starting from the left respect to the FOV of the prototype, the three ^{57}Co planar sources with activity of 429 kBq were placed adjacently. On the right, instead, the three ^{57}Co sources with 143 kBq activity (total activity 429 kBq) were overlapped.

Figure 7. Combination of six planar ^{57}Co sources with 1716 kBq of total activity.

The width of all sources placed next to each other was 32 cm. At 16 cm of distance, the fields of view of the optical and gamma camera are not sufficiently wide to contain all sources shown in figure 7. The distance of 16 cm was decided so that the angular size of the source respect to the prototype was 90°. In this case, at least two measurements were needed, changing the angle of the camera respect to the sources at each time.

Before starting such experiment, we performed an initial measurement at an average distance between the prototype and the sources of 52 cm. This allowed the comparison between the results of the two experiments, and also to observe the response of the camera with such set-up. The results of this first test confirmed the satisfactory performance of the camera in proximity to extended sources (see figure 8 and figure 9), as the line was correctly overlaid using a cut-off threshold of 50%.

Consequently, we performed the originally intended experiment and placed the prototype at 16 cm from the sources, with the same set-up, in order to compare the results of the two experiments.

At an average distance of 16 cm, the data was collected at three different pan angles: −30°, 0°, and 30°, acquiring 180 frames of 1 sec shutter time for each of the three measurement, both in mask and antimask position. The results of such measurements are three gamma images with partially overlapping regions, shown in figure 10.

By observing the results of both figures 9 and 10, the radiation images resulting from the acquisition of 180 frames of 1 sec shutter time do not provide, admittedly, their precise actual shape

2017 JINST 12 P11010

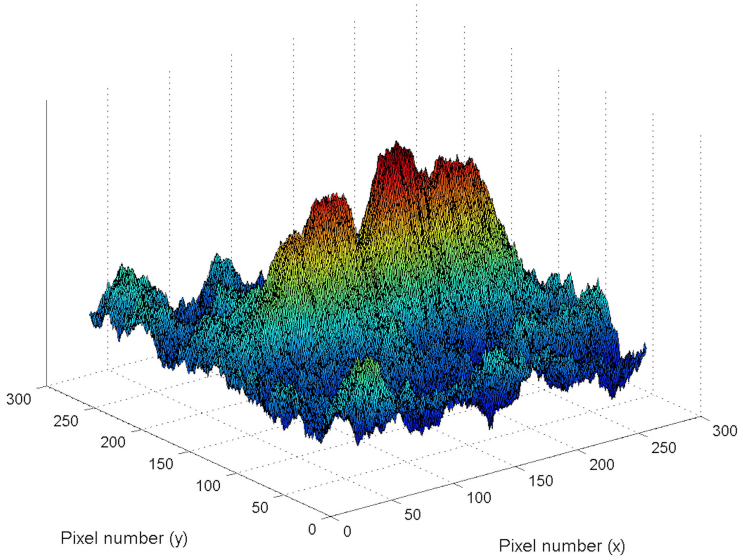

Figure 8. Hotspot profile resulting from the combination of six planar ^{57}Co sources with 1716 kBq of total activity, at an average distance of 52 cm from the gamma camera, providing an ambient dose equivalent rate of ~ 430 nSv/h at the measurement point. As the sources had equal activity, it is possible to notice a loss in counts while approaching the limits of the FOV (see [2] for more details concerning the off-axis response of the gamma camera).

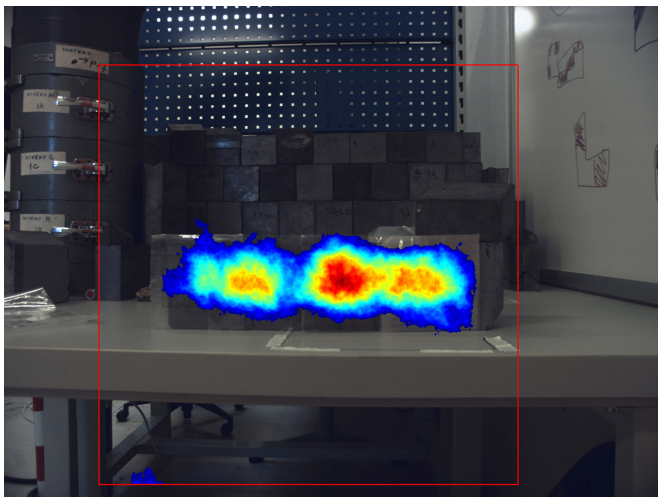

Figure 9. Radiation image superimposed on the respective optical image resulting from the combination of six planar ^{57}Co sources with 1716 kBq of total activity, at an average distance of 52 cm from the gamma camera, providing an ambient dose equivalent rate of ~ 430 nSv/h at the measurement point.

(i.e. equiangular rectangles). A longer acquisition would plausibly have led to a more accurate reconstruction of such shapes. Nonetheless, the results present an amount of details more than sufficient for being correctly interpreted by a human eye.

By applying the radiation image stitching technique described in section 2.2.2, the three γ-images resulting from such experiment have been registered and stitched, resulting into a final coherent composite gamma image, which has been thus superimposed onto its respective optical stitched image. See figures 11 and 12.

2017 JINST 12 P11010

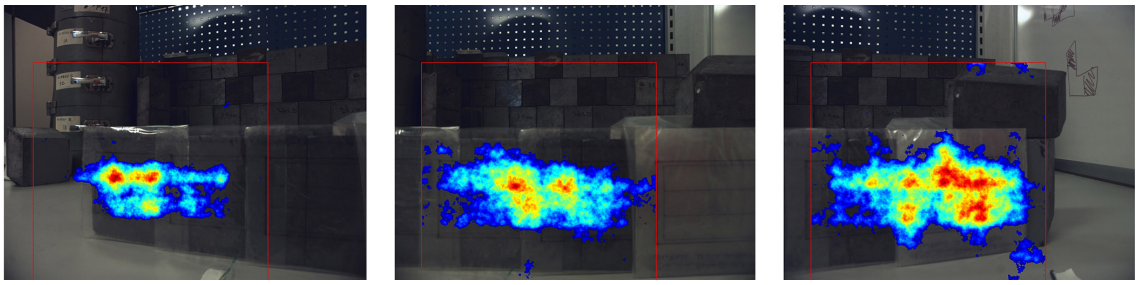

Figure 10. The results of the superimposition of three different measurements performed with the gamma camera prototype, placed at three different pan angles (−30°, 0°, and 30°) from a combination of six planar ^{57}Co sources with 1716 kBq of total activity. The average distance between the sources and the gamma camera was 16 cm, providing an ambient dose equivalent rate of ∼ 530 nSv/h at the measurement point.

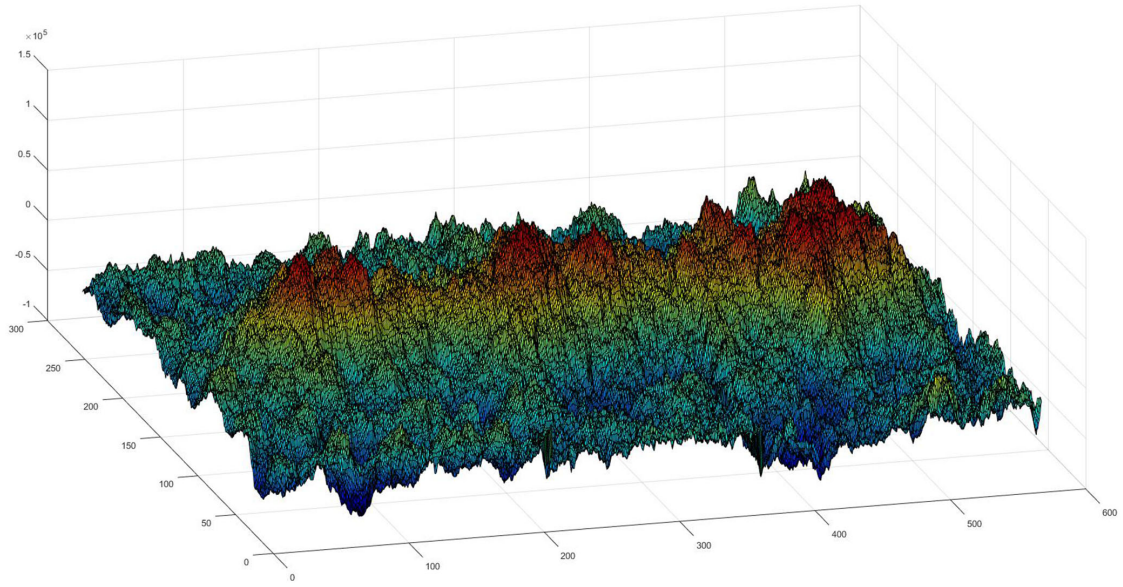

Figure 11. Three-dimensional hotspot profile resulting from the radiation image stitching technique designed and implemented for the prototype. In this example, three radiation images resulting from three different measurements have been combined into a final coherent composite decoded γ-image.

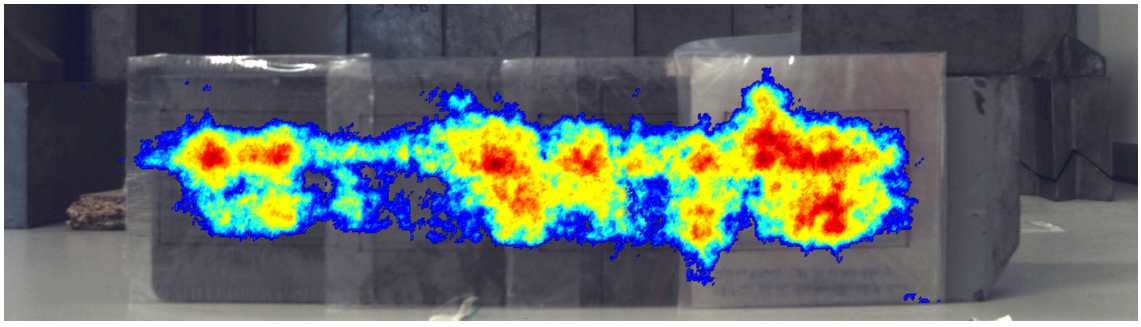

Figure 12. A stitched gamma image resulting from three different measurements superimposed on the respective optical image.

2017 JINST 12 P11010

The hotspot profile and superimposition resulting from the stitching of several decoded gamma images can be then compared with the results of a single measurement performed from a longer distance and shown in figures 8 and 9.

It can be seen that stitching radiation images can offer several advantages. In the first place, if a radioactive source exceeds the FOV of the gamma camera (e.g. long pipes in nuclear power plants), composed panorama γ-images allow the localization of the respective extended surfaces within only one image, preserving though their geometrical coherency.

Moreover, if the surface of a radioactive source needs to be radiologically characterized with accuracy or if its activity is considerably low, panorama gamma imaging allows the possibility of decreasing the distance between the gamma camera and such source, and still being able to localize it entirely within the same image, obtaining thus more detailed radiological information concerning its surface. The result obtained and shown in figure 12 is an example of such scenario, as with equal acquisition time the surface of a low-activity extended source is characterized with more accuracy from a shorter distance.

3.2 Panoramic images with planar and point sources

One of the advantages of panoramic gamma images is that they allow the radiological characterization of entire rooms within one single image, providing an amount of information that can help operators to remember the hotspot position also depending on their location within the interested area.

In order to test a scenario where multiple radioactive hotspots surround an operator, several sources were positioned in the laboratory of CEA Marcoule ("*Laboratoire simulation et techniques de démantèlement nucléaire*"). More specifically, the following sources have been placed at different random locations of the room:

- ^{152}Eu with current activity of 9.63 MBq, at 264 cm from the camera,
- ^{133}Ba with current activity of 9.92 MBq, at 182 cm from the camera,
- ^{241}Am with current activity of 0.15 MBq, at 120 cm from the camera (planar, $12 \times 12\,\mathrm{cm}^2$), and
- ^{137}Cs with current activity of 329 MBq, at 280 cm from the camera.

For each of the sources above mentioned, 300 frames of 1 sec shutter time were acquired using the mask R7e4 in both mask and antimask position, for a total of 600 frames for each source.

In parallel, also the optical images have been captured, covering 360° of the horizontal FOV of the room and ~ 80° of its vertical FOV.

The result of such experiment is shown in figure 13.

The visual details in the γ-images concerning each of the sources mentioned vary inevitably depending on their energy, activity, and their distance respect to the gamma camera. Nevertheless, the radiation images are correctly automatically reprojected and superimposed onto the stitched final optical image without significant artifacts.

In our context, the final images are rendered in spherical coordinates (θ,ϕ), which for this reason is the format accepted by the graphical user interface (GUI) of the prototype for rendering and displaying all stored panorama images. See figure 14.

2017 JINST 12 P11010

Figure 13. A panorama image with size 12574×2316 pixels, with an horizontal and vertical FOV respectively of 360° and 80°, resulting from the stitching of 80 optical images and the superimposition of 4 γ-images. For illustration purposes, the image is shown in black and white.

Figure 14. A screenshot created while rendering via the GUI of the prototype a portion of the panorama image shown in figure 13.

4 Conclusion

A panoramic gamma imaging prototype has been developed, allowing the localization of the main surrounding radioactive sources with a field-of-view of 360 degrees.

Relying on the radiation imaging capabilities of the iPIX gamma camera, a procedure for autonomously obtaining panoramic images with both optical and radiation images has been proposed.

The method for registering and stitching the images generated with the prototype is manly based on ORB, a feature detector and descriptor, in order to compute homographies for the overlapping captured optical images, and it applies, subsequently, the same homographies to their corresponding radiation images.

The results obtained with such method have shown its validity, reconstructing panorama γ-images representing sources that would potentially exceed the FOV of the camera if localized with only one measurement (e.g. long pipes in nuclear power plants), preserving though their geometrical coherency. Moreover, the feasibility of autonomously analysing large rooms or facilities has been proved, displaying the respective result within one single image, thus providing an amount of information that can help operators to remember the hotspot position also depending on their location within the interested area.

All results are displayed via a viewer that has been developed and customized for the gamma camera prototype, allowing the rendering of spherical images and the creation and loading of interactive virtual tours.

2017 JINST 12 P11010

Future perspectives include the validation of the proposed stitching algorithm by performing additional measurements involving large radioactive sources in real-life scenarios. Moreover, the implemented algorithm relies on the assumption that no occluding objects are present between the located sources and the instrument. Such limitation is due to the inherent low spacial resolution of the images obtained with the current version of the gamma camera. Improvements related to such aspect may lead in the future to the possibility of stitching gamma images relying only (or, at least, partially) on the visual features of the radiation images, such as corners or edges of the located radiation-emitting objects.

Furthermore, the current version of the algorithm makes only partial use of the Nvidia CUDA libraries [19]. The associated computational performances may be improved by relying more on the multiple cores of the graphics processing unit (GPU) of the computing board used, and by further optimizing its pipeline [1].

References

[1] M. Adam, C. Jung, S. Roth and G. Brunnett, *Real-time Stereo-Image Stitching using GPU-based Belief Propagation*, in *Vision, Modeling, and Visualization Workshop*, pg. 215–224 (2009).

[2] K. Amgarou et al., *A comprehensive experimental characterization of the iPIX gamma imager*, 2016 *JINST* **11** P08012.

[3] P. Baudisch et al., *Panoramic viewfinder: providing a real-time preview to help users avoid flaws in panoramic pictures*, in *Proceedings of the 17th Australia conference on Computer-Human Interaction: Citizens Online: Considerations for Today and the Future*, pg. 1–10, Computer-Human Interaction Special Interest Group (CHISIG) of Australia (2005).

[4] K. Biswas and M. Du, *What causes high resistivity in CdTe*, *New J. Phys.* **14** (2012) 063020 [arXiv:1202.2255].

[5] G. Bradski and A. Kaehler, *Learning OpenCV: Computer vision with the OpenCV library*, O'Reilly Media, Inc. (2008).

[6] M. Brown and D.G. Lowe, *Automatic Panoramic Image Stitching using Invariant Features*, *Int. J. Comput. Vision* **74** (2007) 59.

[7] M. Calonder, V. Lepetit, C. Strecha and P. Fua, *BRIEF: Binary robust independent elementary features*, in *Computer Vision — ECCV 2010*, Lecture Notes in Computer Science, vol. 6314, pg. 778–792, Springer, Berlin, Heidelberg (2010).

[8] C. Chen and R. Klette, *Image stitching — comparisons and new techniques*, in *Computer Analysis of Images and Patterns — CAIP 1999*, Lecture Notes in Computer Science, vol. 1689, pg. 835–835, Springer, Berlin, Heidelberg (1999).

[9] S.E. Chen, *Quicktime VR: An image-based approach to virtual environment navigation*, in *Proceedings of the 22nd annual conference on Computer graphics and interactive techniques*, pg. 29–38 (1995).

[10] M.J. Cieślak, K.A.A. Gamage and R. Glover, *Coded-aperture imaging systems: Past, present and future development — a review*, *Radiat. Meas.* **92** (2016) 59.

[11] R.H. Dicke, *Scatter-Hole Cameras for X-Rays and Gamma Rays*, *Astrophys. J.* **153** (1968) L101.

[12] S. Dubos et al., *ORIGAMIX, a CdTe-based spectro-imager development for nuclear applications*, *Nucl. Instrum. Meth.* **A 787** (2015) 302 [arXiv:1502.01491].

2017 JINST 12 P11010

[13] Future Technology Devices International Ltd., *D2XX drivers for FTDI devices*, http://www.ftdichip.com/Drivers/D2XX.htm (2016), accessed: 2 January 2017.

[14] O. Gal et al., *Development of a portable gamma camera with coded aperture*, *Nucl. Instrum. Meth. A* **563** (2006) 233.

[15] J. Gallier, *Basics of Projective Geometry*, in *Geometric Methods and Applications*, Texts in Applied Mathematics, vol. 38, Springer, New York, NY (2011).

[16] M. Gmar, M. Agelou, F. Carrel and V. Schoepff, *GAMPIX: A new generation of gamma camera*, *Nucl. Instrum. Meth. A* **652** (2011) 638.

[17] S.R. Gottesman and E.E. Fenimore, *New family of binary arrays for coded aperture imaging*, *Appl. Opt.* **28** (1989) 4344.

[18] N. Greene, *Environment mapping and other applications of world projections*, *IEEE Comput. Graph. Appl.* **6** (1986) 21.

[19] M. Harris, *Many-core GPU computing with NVIDIA CUDA*, in *Proceedings of the 22nd annual International Conference on Supercomputing (ICS)*, pg. 1, ACM (2008).

[20] R. Hartley and A. Zisserman, *Multiple view geometry in computer vision*, Cambridge University Press (2003).

[21] D. Hill, P.G. Batchelor, M. Holden and D.J. Hawkes, *Medical image registration*, *Phys. Med. Biol.* **46** (2001) R1.

[22] V. Kraus, M. Holik, J. Jakubek, M. Kroupa, P. Soukup and Z. Vykydal, *FITPix: Fast interface for Timepix pixel detectors*, 2011 *JINST* **6** C01079.

[23] H. Lemaire, *Développement d'une caméra gamma de troisième génération*, Ph.D. Thesis, University of Caen Normandy (2015).

[24] X. Llopart, R. Ballabriga, M. Campbell, L. Tlustos and W. Wong, *Timepix, a 65k programmable pixel readout chip for arrival time, energy and/or photon counting measurements*, *Nucl. Instrum. Meth.* **A 581** (2007) 485 [*Erratum ibid.* **A 585** (2008) 106].

[25] D.G. Lowe, *Distinctive image features from scale-invariant keypoints*, *Int. J. Comput. Vision* **60** (2004) 91.

[26] B.D. Lucas and T. Kanade, *An Iterative Image Registration Technique with an Application to Stereo Vision*, in *Proceedings of the 7th International Joint Conference on Artificial Intelligence*, pg. 674–679 (1981).

[27] J.B. Maintz and M.A. Viergever, *A survey of medical image registration*, *Med. Image Anal.* **2** (1998) 1.

[28] H. Marcus and H. Hermann, *Heterogeneity by the Numbers: A Study of the ODROID XU+E big.LITTLE Platform*, in *6th Workshop on Power-Aware Computing and Systems (HotPower 14)* (2014).

[29] D. Matsuura, K. Genba, Y. Kuroda, H. Ikebuchi and T. Tomonaka, *ASTROCAM 7000HS Radioactive Substance Visualization Camera*, *Mitsubishi Heavy Industries Technical Review* **51** (2014) 68.

[30] J. Pluim, J.B. Maintz and M.A. Viergever, *Mutual-information-based registration of medical images: a survey*, *IEEE Trans. Med. Imag.* **22** (2003) 986.

[31] I.E. Richardson, *H. 264 and MPEG-4 video compression: video coding for next-generation multimedia*, John Wiley & Sons (2004).

2017 JINST 12 P11010

[32] E. Rosten and T. Drummond, *Machine learning for high-speed corner detection*, in *Computer Vision — ECCV 2006*, Lecture Notes in Computer Science, vol. 3951, pg. 430–443, Springer, Berlin, Heidelberg (2006).

[33] E. Rublee, V. Rabaud, K. Konolige and G. Bradski, *ORB: An efficient alternative to SIFT or SURF*, in *IEEE International Conference on Computer Vision (ICCV)*, pg. 2564–2571 (2011).

[34] B. Smith et al, *A new look at the saturn system: The voyager 2 images*, *Science* **215** (1982) 504.

[35] B.A. Smith et al, *The Jupiter system through the eyes of Voyager 1*, *Science* **204** (1979) 951.

[36] S. Sun et al, *Development of a panorama coded-aperture gamma camera for radiation detection*, *Radiat. Meas.* **77** (2015) 34.

[37] R. Szeliski and H. Shum, *Creating full view panoramic image mosaics and environment maps*, in *Proceedings of the 24th annual conference on Computer graphics and interactive techniques*, pg. 251–258 (1997).

[38] T. Takahashi and S. Watanabe, *Recent progress in cdte and cdznte detectors*, *IEEE Trans. Nucl. Sci.* **48** (2001) 950 [astro-ph/0107398].

[39] M. Woodring et al., *Advanced radiation imaging of low-intensity gamma-ray sources*, *Nucl. Instrum. Meth. A* **422** (1999) 709.

[40] B. Zitova and J. Flusser, *Image registration methods: a survey*, *Image Vision Comput.* **21** (2003) 977.

2017 JINST 12 P11010